Scientific Journal for the Faculty of Science-Sirte University Vol. 5, No. 1 (2025) 93-102

Scientific Journal for the Faculty of Science-Sirte University

Journal home page: http://journal.su.edu.ly/index.php/JSFSU/index

DOI: 10.37375/issn.2789-858X

Fibrous Cerium Phosphate and its Intercalated-Urea Product as Versatile Adsorbents for Mercury (II) Removal

Souad M. Kshed[1], Hana B. A. AlHanash[1], Ragiab A. M. Issa[2*]

[1]*Libyan Advanced Center for Chemical Analysis, Libyan authority for scientific research Tajoura, Libya*

[2]*Chemistry department, Faculty of Education, University of Tripoli, Tripoli, Libya*

DOI: https://doi.org/10.37375/sjfssu.v5i1.3199

ARTICLE INFO:

Received 31 January 2025.

Accepted 03 April 2025.

Published 17 April 2025

Keywords:

Adsorption; fibrous cerium phosphate; isotherm; mercury ion; urea.

A B S T R A C T

Fibrous Nano cerium Phosphate was achieved by reacting Cerium Sulphate solution with phosphoric acid at 80°C for several hours. Furthermore, Urea was intercalated into the prepared f-cerium phosphate. Techniques like Fourier Transform Infra-Red spectroscopy, X-ray diffraction, Scanning Electron Microscope, and Thermogravimetric analysis were used to characterize these products. Under various conditions, the products were examined to their adsorption capability to extract mercury (II) ions from aqueous solution. The semicrystalline nature of the phosphates was demonstrated by XRD, and the interlayer d-spacings for the cerium phosphate and urea-intercalated compounds were 10.6 and 11.3 Å, respectively. The FTIR spectra of the intercalated phosphate showed an additional peak at 1400 cm^{-1} corresponding to C-N stretching confirming the presence of urea. The SEM showed a fibrous morphology of the cerium phosphate with a particle size of 16µm. The optimum adsorption conditions were at pH values 3.0 at a reaction time interval of 30 minutes. Pure cerium phosphate behaved differently from intercalated cerium phosphate, which consistently showed a decrease in adsorption percentage as the initial ion concentration increased. Both phosphates showed a systematic increase in adsorption percentage as the adsorbent amount increased, however, pure cerium phosphate showed greater adsorption ability than its intercalated analogue. Both Freundlich and Langmuir isotherm models were used, and their linearity curves are comparable. For pure and intercalated chemicals, the Langmuir model yielded R^2 values of 0.5351 and 0.7283, respectively. According to the Freundlich model, the pure and intercalated phosphates R^2 values were 0.5823 and 0.8649 respectively. Although a low correlation is observed, the intercalated material fit both isotherms and showed a slightly better behaviour.

1 Introduction

Around the world, water contamination has become a major problem. As the population grows, industry develop rapidly, agriculture practices increase and environmental changes occur, the quality of water sources become increasingly crucial (Zeng et al., 2011). The continuous release of different pollutants into the environment, such as heavy metals, organic chemicals, and radioactive substances, caused a significant global issue (Ghasemi et al., 2019). The removal of heavy and harmful substances from water is a significant environmental issue that receives a lot of attention (Doğan et al., 2008). Adsorption is regarded as a quick and reasonably economical method for treating water

Corresponding author: E-mail: ra.issa@uot.edu.ly

and wastewater since it is simple and ecofriendly method (Deng et al., 2013).

As a result of the discharge of wastewater and flue gas from different industries such as plastic, battery, and electronic industries, mercury can be widely distributed in the soil, the atmosphere, and water resources. Mercury is highly transferable, bio-accumulative, and poisonous. Chromosome variation, birth defects, neurological damage, and renal poisoning are all possible outcomes of mercury exposure (Duan et al., 2018). Mercury is therefore classified as a priority hazardous contaminant. In many nations throughout the world, the limits for mercury in drinking water and wastewater are set at 1 mg L^{-1} (Gao et al., 2023) and 50 mg L^{-1} (Kumar and Singh., 2021), respectively. Therefore, bringing the mercury levels down below the safety threshold is crucial.

Numerous adsorbents, including clays, metal oxides, and certain organic and inorganic ion exchangers, have been reported to remove different types of contaminants from water and wastewater. Chitosan was successfully used to remove uranium, mercury and other pollutants from water (Michailidou et al., 2021). Al-Ghouti et al. (2019) using date pits in removing mercury from water. Montmorillonite clay and some of its intercalates have been used for the removal of mercury from its aqueous solution (Guerra, et al., 2009). Cysteine polyacrylonitrile (sPAN) fiber has been used (Duan et al., 2018) for removing high concentrations of mercury (20-500 mgL^{-1}) from its aqueous solution. According to the US Environmental Protection Agency (EPA) and the World Health Organization (WHO), the maximum permissible mercury level in drinking water is 0.001-0.002 mgL^{-1} (Ebrahimi et al., 2012).

The goal of this work is to synthesize fibrous nanocerium phosphate and its urea intercalate and study their ability to remove low mercury ion concentrations from aqueous solutions under different conditions.

2 Materials and Methods

2.1 Materials and equipments

All used chemicals were analytical grade reagents: Cerium sulphate tetrahydrate (Merck 98%); Urea (Riedel-de Haen); Orthophosphoric acid (Reachim, 85%); Sulphuric acid (Carlo Erba 96%); Sodium Hydroxide (Merck 99.5%); Potassium chlorate (Riedel-de Haen 99%); Potassium Perchlorate (Laboratory reagent T-baker lab chemicals); Potassium Chloride (Merck). Hydrochloric acid (BDH). Mercury standard solution (1000ppm) was from (Merck).

Mercury analyzer model (lab Analyzer 254), FTIR Agilent; XRD Philips (PW 1800); TGA, Labodam; SEM, (JSM- 5610LV) JEOL.

2.2 Preparation of starting materials

At 80˚C, 300 ml of 6 M phosphoric acid was added with 300 ml of 0.05M cerium sulfate solution (in 0.5M H_2SO_4 solution) dropwise. The mixture was stirred for four hours. The resulting substance was then stirred for an hour at 60˚C after being dispersed in 3 litters of hot distilled water. The final product, was thoroughly washed with distilled water several times till pH 3, filtered and air dried shown as a sheet in Figure (1.a).

2.3 Intercalation of urea

0.25 g of cerium phosphate were dispersed in 100 ml of 0.1 M urea and kept stirring for 72 hours at room temperature, then filtered and dried (Figure 1b)

2.4 Adsorption experiments

Unless the ion concentration is the parameter to study, 30 mL of 5 ppb mercury (II) ion (Hg^{2+}) solution were transferred into a 50 mL centrifuge tube. The pH was adjusted to 3.0, and then 0.06 g of the adsorbent material was added, and the volume was completed to 40 mL with deionized water. The solution was then kept shaking for 3 hrs, followed by centrifugation, a clear aliquot was collected in a clean plastic tube for mercury analysis. Similarly, the effect of adsorbent amount was studied by repeating the steps above except for using different amounts of adsorbent at the same conditions throughout the experiment. Whereas in the case of pH effect, similar experiment was implemented as above at different pH value (1 to 8), keeping constant initial ion concentration, 5 ppb Hg^{2+} (Alhanash H. B. et al., 2022)

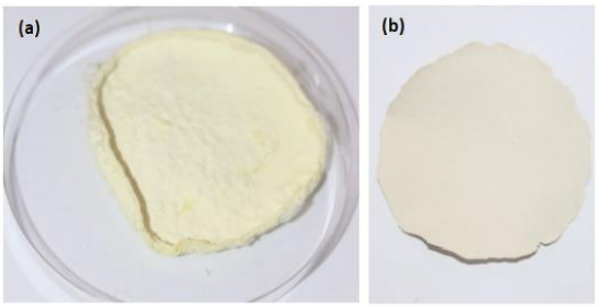

Figure 1. Photo Images for CeP (a) and urea-CeP (b)

3 Results

3.1 Characterization of the product

FTIR: The synthesized cerium phosphate and its urea intercalation were characterized using different techniques such as FTIR, XRD, TG, and exchange capacity. Fig. 2 shows the FTIR spectra for both pure and urea intercalated fibrous CeP. These spectra resemble those of the tetravalent metal phosphate, with the broad curve at 3328 cm^{-1} signifying the N-H groups and interlayer water molecules. The asymmetric P-OH group, which stands for the phosphate group's stretching vibration and the H-O-H group's bending vibration, is responsible for the curves at 1620 cm^{-1} (Wang et al., 2023). The phosphate group's vibrations (symmetric and asymmetric P-O stretching) are the cause of the broad, steep curve in the 1237-917 cm^{-1} range. The Ce-O bond vibrations are specifically represented by the curve in the 600–500 cm^{-1} range (Zhao et al., 2022). The presence of carbonyl and amide groups is indicated by the additional peaks in the urea-intercalated cerium phosphate's infrared spectra at 1650 cm^{-1} and 1400 cm^{-1}.

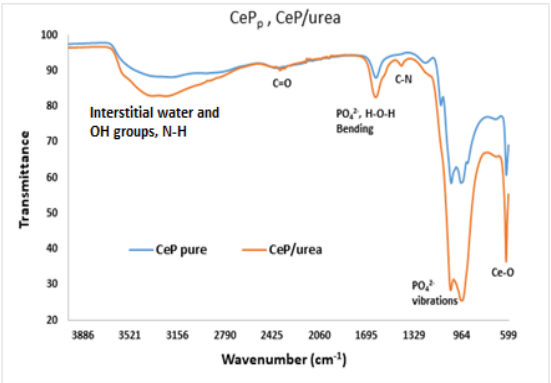

Figure 2. FTIR spectrum for pure CeP and CeP/urea

The rise in the intensity of hydrogen bond absorption further confirms that the intercalation of urea into the cerium phosphate fibrous structure was successful.

XRD: The PW 1800 X-ray diffractometer, with Cu Kα radiation (1.5406 Å) generated at 40 kV and 30 mA, respectively. X-ray data related to angle 2□ from 2 to 80 were collected using X'Pert Industry Software.

Fig. 3. shows the X-ray diffraction pattern for CePf, indicating a diffraction maximum with an interlayer spacing of d001 = 10.76 Å, consistent with what was previously reported (Wang et al., 2023) and a semi-crystalline structure. From the data obtained for fibrous cerium phosphate, the crystallite size was found to be 10.6 nm. Fig. 3 also shows the X-ray diffraction pattern for CeP/urea. The XRD results of the fibrous cerium phosphate complex after urea intercalation show a remarkable change in the crystal structure with an increase in the interlayer spacing from 10.7 to 11.13 Å, an indication that the urea intercalation successful, which led to an increase in the interlayer spacing value by 0.43 Å. In addition, there are additional curves at 11.7346, 17.9097, 28.3387, 34.4903, and 50.8767 (°2□) due to the presence of a urea compound, which led to a change in the crystal structure of the intercalated complex.

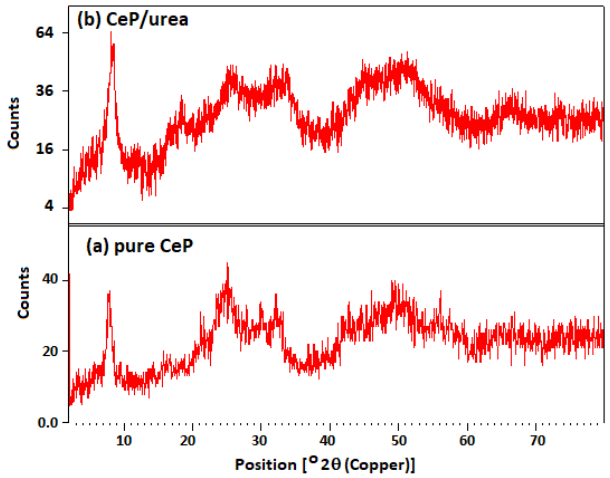

Figure 3. XRD patterns for pure (a) and urea (b) intercalated cerium phosphate

SEM: The scanning electron microscope image shows a network (Fig. 4 a & b) of interconnected fibers, very fine fibres with a uniform and interwoven distribution and

high porosity that enhances the surface area required for chemical reactions. The interconnected fibers form a three-dimensional network with high porosity, which enhances the effective surface area, making the material suitable for applications requiring a large surface area, such as ion exchange, chemical adsorption, and chemical catalysis.

TEM: image of the nanosized fibrous cerium phosphate (nCePf) is shown in Fig. 4-c, with an average rod size around 100nm length and 10nm thickness.

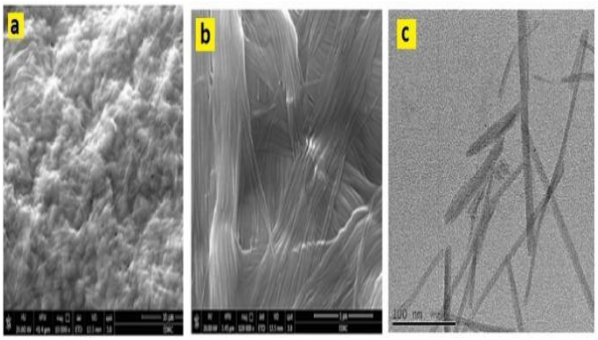

Figure 4. SEM (a & b) and TEM (c) images for pure cerium phosphate

The scanning electron microscope (SEM) image of the urea-intercalated cerium phosphate compound shows a significant change when compared to pure fibrous cerium phosphate, as the fibers are not uniform and distributed randomly, with irregularly shaped particles all over the fibrous network. The average crystallinity according to SEM data was calculated and found to be 16 nm. These particles represent the urea compound intercalated within the cerium phosphate network; see **Fig. 5**.

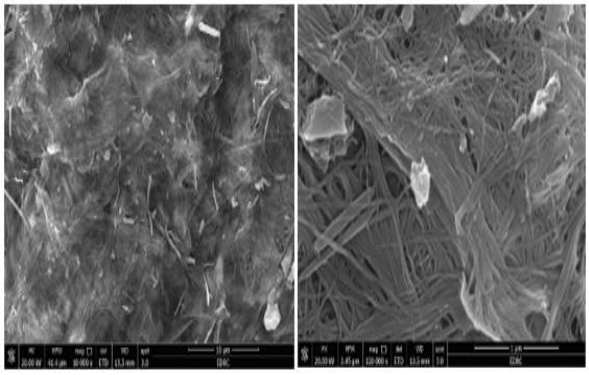

Figure 5. SEM Image for urea intercalate cerium phosphate

TGA: The thermal analysis diagrams of the pure fibrous cerium phosphate (CePf) and cerium phosphate intercalated with urea (CePf/urea) are displayed in Fig. 6. The thermal decomposition of fibrous CeP happens in multiple stages. The first stage involves the loss of surface water molecules and some volatile organic species from 25 to 180 °C, 16.27% loss, followed by the condensation of POH groups in various stages. Cerium pyrophosphate (CeP2O7) is thought to be the resulting end product from this behaviour, and the overall weight reduction was 27.32%.

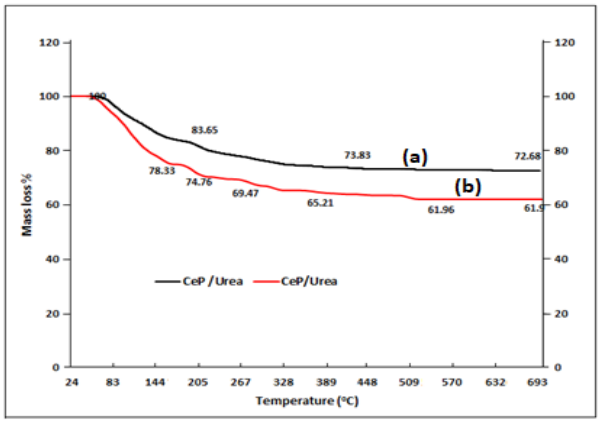

Figure 6. TGA thermograms for CeP and CeP/urea

A total weight loss of 38.1%, is shown in the thermal decomposition of CeP/urea, which took place in multiple steps. The first step involves the loss of surface water molecules from 25 to 145 °C, or 16.27%. This is followed by the condensation of POH groups in various steps with the breakdown of organic matter (Shakshooki, 2014). Because urea was present, the overall loss of urea-intercalated fibrous cerium phosphate was 10.78% greater than that of pure fibrous cerium phosphate.

Exchange capacity: A known amount of fibrous cerium phosphate was immersed in a NaCl solution of known concentration, and the suspension was titrated against a 0.1M NaOH solution at intervals of 0.5mL (AlHanash et al., 2022) while stirring, as observed in **Fig. 7**. Ultimately, the curve revealed that the exchange capacity was as expected 4.25 meq. g^{-1}.

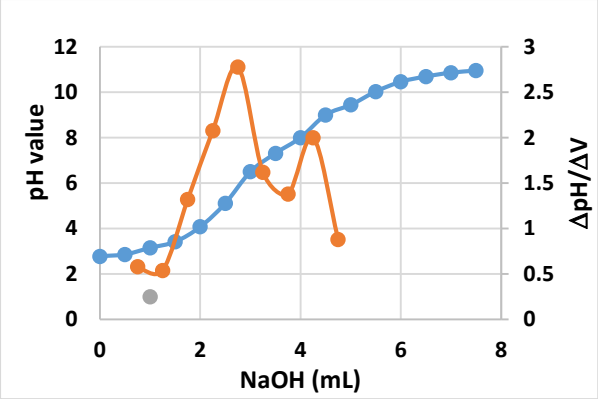

Figure 7. Exchange capacity of pure cerium phosphate

3.2 Adsorption procedures

Mercury Analyzer (lab Analyzer 254) *was* used to measure the concentration of mercury (Hg^{2+}) in all batch experiment solutions at low concentration (1-5 mg/L). The obtained curve (Fig 8) was linear obeying beer's law with an equation; $y = 0.0501x + 0.0002$ and a correlation coefficient $R^2 = 0.998$. The limit of detection (LOD) was calculated accordingly and found to be 0.306 mg. L-1.

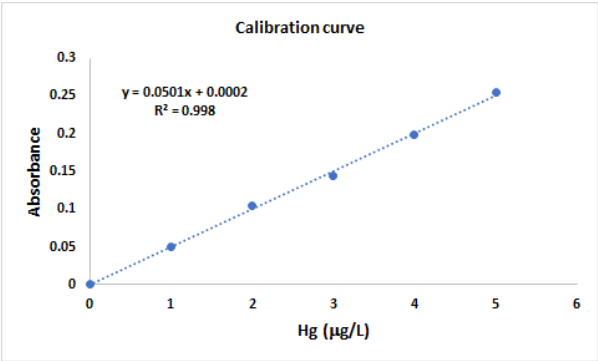

Figure 8. Mercury ion calibration curve

3.2.1 Effect of contact time

Fig. 9 illustrates the effect of contact time on Hg^{2+} ion adsorption by cerium phosphate. In the first 20 minutes, adsorption rapidly increases from about 84% to 98%, driven by abundant active sites on the fibrous CeP surface. This process involves both physical (van der Waals forces) and chemical interactions (covalent or ionic bonds). After 20 minutes, the adsorption plateaus at approximately 98% as active sites approach saturation, leading to a gradual decrease in the adsorption rate and establishing a dynamic equilibrium between adsorbed and remaining mercury ions (Bash et al., 2007; Youssif et al., 2024). From 20 to 100 minutes, the adsorption remains stable at 98%, indicating equilibrium, where no further mercury ion adsorption occurs. The optimal contact time for maximum adsorption is thus 20 minutes, after which extending the time is unnecessary.

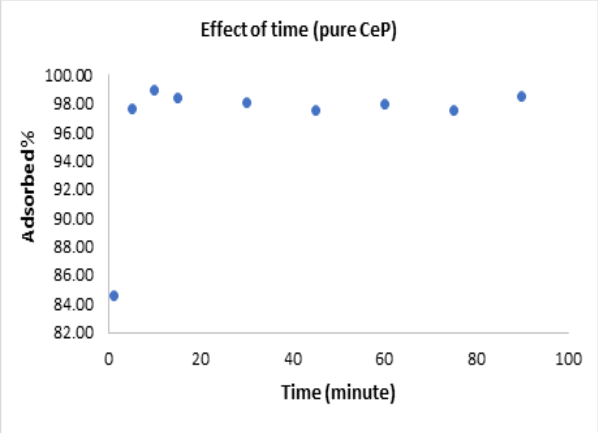

Figure 9. Effect of contact time on the adsorption of mercury ions on CeP

3.2.2 Effect of pH

Fig. 10. shows the effect of pH on the adsorption of mercury ions using CeP, this may be explained in different stages, at low pH (1-2) values, the adsorption percentage ranges between 30-50%, in strong acidic medium there is a high competition of H^+ ions and Hg^{2+} ions to the active sites resulting in reduction of the adsorption efficiency. The adsorption percentage increases gradually to about 90% at pH 2-4, due to the decrease in concentration of H^+ ions which reduces the competition with mercury ions. At this stage, the surface-active sites of adsorbent become optimally charged to interact and bind with mercury ions. The less acidic medium enhances the stability of mercury ions, facilitating their adsorption on the surface. At this stage, chemisorption may play a greater role than physical adsorption (Michailidou et al., 2021). Whereas, above pH 4 adsorption percentage is relatively stable due to the precipitation of Hg2+ as hydroxides, such as $Hg(OH)_2$ leading to a reduction in the mercury ions concentration in the solution. This leads to a decrease in adsorption

efficiency of the pure CeP, similar behaviour is reported previously (Al-Ghouti et al., 2019).

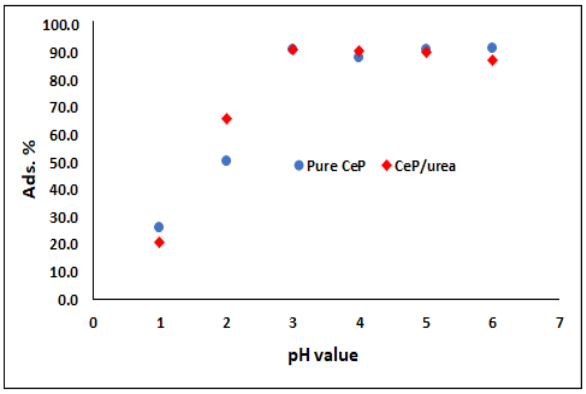

Figure 10. Effect of pH on the adsorption of Hg^{2+} on CeP and CeP/urea

Fig. 10 shows the effect of pH on mercury ion adsorption by CeP-Urea. At pH 1, adsorption is only 20% due to strong competition from H^+ ions for adsorption sites. As pH increases from 2 to 4, adsorption rises sharply, reaching about 70% at pH 2 and exceeding 90% at pH 3-4, as H^+ ion concentrations decrease. This enhances adsorption due to more available sites on cerium phosphate. At pH 5-6, adsorption remains stable because mercury ions precipitate as hydroxides, reducing their solution concentration and lowering adsorption efficiency (Qasem et al., 2021).

3.2.3 Effect of initial ion concentration

With both pure cerium phosphate and cerium phosphate intercalated with urea, the influence of the initial concentration of the mercury ion on adsorption was investigated. Mercury ions were present in different concentrations between 0.5 and 3.5 parts per billion. At low mercury ion concentrations (0.5-1.5 ppb), the percentage of mercury ion removal from the solution by cerium phosphate dropped from 99% to roughly 54% when the initial ion concentration was between 0.5 and 1.5mg/L (Fig. 11). The control mechanism responded differently from what is known at higher concentrations (2-2.5 ppb). At concentrations between 2.5-3.5 mercury ions, the system tended to be nearly fictitious. Since it is now present in ions with negative organic sites on the adsorbent surface, this is necessary for the adsorption of cations on the adsorbent surfaces (Michailidou et al., 2021). Conversely, as the ion concentration increased from 0.5 to 3.5 ppm, the adsorption percentage on the surface of cerium phosphate and urea increased from 84% to almost 97%.

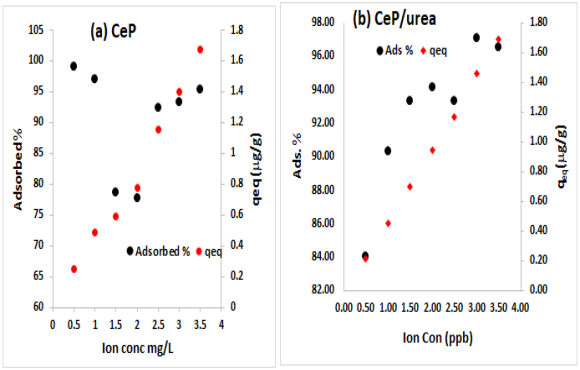

Figure 11. Effect of initial ion concentration on the adsorption of Hg^{2+} on CeP (a) and CeP/urea (b)

As the mercury ion concentration rose from 0.5 to 3.5 ppm in both situations, the adsorption capacity increased steadily. In both instances, the adsorption capacity rose from roughly 0.2 to roughly 1.7 µg/g.

3.2.4 Effect of the adsorbent amount

Fig. 12 depicts the effect of adsorbent amount (CeP and CeP/urea) on mercury ion adsorption. As the adsorbent quantity increases, the available surface area also increases, leading to a rise in adsorption percentage. This trend continues until it plateaus, typical of physical adsorption, which relies on interactions without chemical bonds (Aljamali et al., 2021). Adsorption capacity (q_e), defined as mg Hg^{2+}/g adsorbent, decreases with higher adsorbent concentrations. Since mercury ion concentration remains constant, not all active sites are utilized, reducing q_e. This suggests that excess adsorbent can diminish effectiveness (Abdel-Hady et al., 2023). At low adsorbent concentrations, chemical adsorption predominates as mercury ions quickly occupy limited active sites. Conversely, at higher concentrations, physical adsorption increases due to more available surface sites. However, the increase in adsorbent does not linearly correlate with adsorbed molecules, leading to a decrease in q_e (Aljamali et al., 2021). Saturation occurs at high adsorbent amounts, stabilizing Ads. %. An optimal adsorbent amount must be chosen based on mercury ion concentration and active site availability.

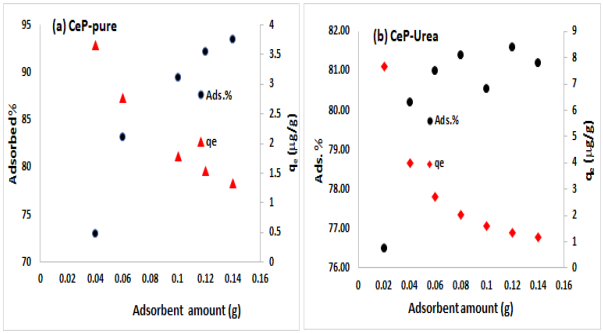

Figure 12. Effect of adsorbent amount on the adsorption of Hg^{2+} on CeP (a) and CeP/urea (b)

Fig. 12. illustrates the relationship between adsorbent amount, total adsorption percentage (Ads. %), and adsorption capacity (q_e) for mercury adsorption on urea-intercalated cerium phosphate. As adsorbent quantity increases, Ads. % increases gradually due to the availability of more active sites until it reaches saturation.

The equilibrium adsorption capacity (q_e) reflects the mg (Hg^{2+})/ g (adsorbent). With more adsorbent, mercury ions are distributed over a larger area, causing q_e to decline as some active sites remain unused. At saturation, Ads. % stabilizes, making the mercury concentration the primary factor in adsorption.

Physical adsorption prevails at higher adsorbent amounts, relying on surface area rather than completely utilized active sites. In contrast, chemical adsorption is more significant at lower amounts due to interactions between functional groups from urea modification and mercury ions. While urea enhances cerium phosphate's performance, it does not prevent the decrease in q_e with increased adsorbent quantity (Issa et al, 2023).

3.3 Modelling isothermal

Batch experiments produced an equilibrium curve for mercury ions. At pH 4.5 with 5 ppb mercury, cerium phosphate and urea-intercalated cerium phosphate were added in varying amounts (0.5 to 5.3 g/L). The Langmuir curve (Equation 3-1) was used to calculate adsorption capacity in mg per g of adsorbent. The Freundlich model, applicable to both chemisorption and physical adsorption, describes adsorption on heterogeneous surfaces and is effective at low to intermediate concentrations (Boparai et al., 2011). Equation (3-2) represents the linear Freundlich equation.

$$q_e = \frac{C_o - C_e}{m(g)} \times V(L) \qquad (3-1)$$

$$\log(q_{max}) = \log(K_F) + \frac{1}{n}\log(C_o) \quad (3-2)$$

The adsorption process of mercury ions on both materials was subjected to modeling using several mathematical models such as the Langmuir line and the Freundlich line. These processes showed the following results:

3.3.1 Langmuir isotherm

The maximum adsorption capacity of mercury ions on cerium phosphate metal is represented by q_{max} (mg/g), and the constant K_L (L/mg) describes the attraction between the adsorbent (metal ion) and the adsorbent (metal). Equation 3-3 was used to apply the Langmuir model to describe the isotherm. The Langmuir model is linearized in Equation 5-3 with a low correlation coefficient R^2=0.5351 for cerium phosphate and is better and more linear for cerium phosphate intercalated with urea, where R^2=0.7283 (Langmuir, 2018; Suleyman, 2020). The basis of this concept is the hypothesis-supported by Langmuir theory-that adsorption occurs in specific homogeneous regions within the adsorbent.

$$\frac{C_e}{q_e} = \frac{C_e}{q_{max}} + \frac{1}{q_{max} \times K_L} \qquad (3-3)$$

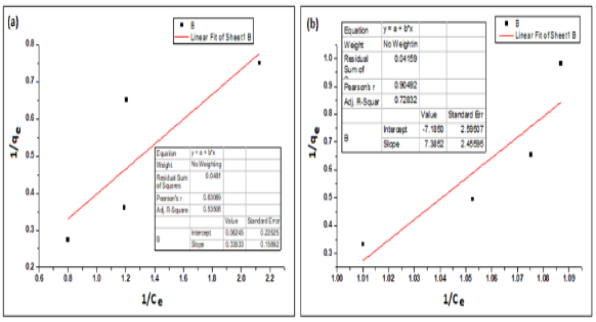

Figure 13. Langmuir isotherm for the adsorption of on CeP (a) and CeP/Urea (b)

By fitting the plot of 1/qe versus 1/Ce (**Fig. 13**), the Langmuir constant (K_L) was calculated using the slope and intercept of the linear equation (Eq. 3.4); see Eqs. 3-5 and 3-6. The maximum adsorption capacity (q_{max}) for pure cerium phosphate was found to be 2.98 µg/g, while it was 0.135 µg/g, for cerium phosphate intercalated with urea. In this work, the Langmuir constant was found to

be 5.37 L/mg for pure cerium phosphate, while it was -1.031 L/mg for cerium phosphate intercalated with urea. The adsorption of mercury ion (Hg^{2+}) at high concentrations (5-50 mg. L^{-1}) on both polyaniline (PA) and polyvinyl aniline (PVA) was studied, and the Langmuir isotherm was applied, which gave a good linear relationship (Zhangtao et al., 2017).

$$y = mx + c \qquad (3-4)$$

$$q_{max} = \frac{1}{slope} \qquad (3-5)$$

$$K_L = \frac{1}{q_{max} \times intercept} \qquad (3-6)$$

$$R_L = \frac{1}{1+C_o \times K_L} \qquad (3-7)$$

The separation factor RL was calculated using Eq. 3-7 and was found to be 0.037 for pure cerium phosphate and -0.241 for urea-intercalated cerium phosphate, where KL is the Langmuir constant and Co is the initial concentration. According to McKay et al. (1982), the value of RL indicates the type of the Langmuir thermodynamic curve as irreversible ($R_L = 0$), linear ($R_L = 1$), unfavorable ($R_L > 1$), or favorable ($R_L > 1$) (0). Therefore, the Langmuir model in our case shows that the Langmuir thermodynamic curve is favorable for this experiment for pure cerium phosphate, while it is negative for urea-intercalated cerium phosphate. A negative K_L value means that different (heterogeneous) parts of the adsorbent interact negatively with the surface of the adsorbent, resulting in desorption rather than adsorption.

However, according to some studies, the Langmuir model tries to describe the attractive interactions that occur when molecules of the absorbent substance are drawn to the surface adsorption sites, as some researchers have already explained (Perwitasari et al., 2021). When comparing the Langmuir model's output with the experimental findings (refer to **Figs. 8 and 9**), we discover that:

	q_{eq}	q_{max}	R^2	K_L	R_L
Pure CeP	3.65	2.98	0.5351	5.33	0.036
Urea-CeP	7.65	0.14	0.7283	-0.01	0.011

3.3.2 Freundlech isotherm

Fig. 14 shows the effect of the Freundlich isothermal model of mercury ions on both pure cerium phosphate (a) and urea-intercalated cerium phosphate (b). The adsorption results appear to be well represented by the Freundlich model, as evidenced by the correlation coefficient (R^2) for pure cerium phosphate of 0.5821 and for urea-intercalated cerium phosphate $R^2 = 0.8649$. The Freundlich constant KF indicates the Freundlich adsorption capacity, and n characterizes the heterogeneity of the system as suggested by some researchers (Akl, 2021). These values are calculated from Eqs. 3-8 and 3-9.

$$\frac{1}{n} = slope \qquad (3-8)$$

$$logK_F = intercept \qquad (3-9)$$

Our work describes the behaviour of mercury ions on cerium phosphate (a) and urea-intercalated cerium phosphate (b) during monolayer and multilayer adsorption. The KF of cerium phosphate mineral was determined to be (2.673 (mg/g)*(L/mg)1/n) and 1/n was found to be 2.283 from Figure 3.3.2. The Freundlich constant for cerium phosphate intercalated with urea was (3.661 (mg/g)*(L/mg)1/n) and the value of 1/n was 0.170, indicating that a chemical adsorption has occurred.

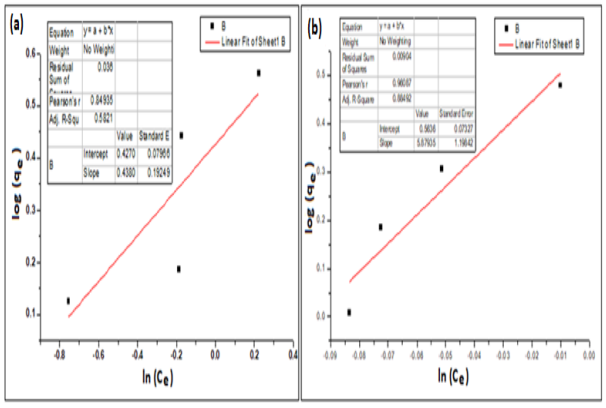

Figure 14. Freundlich isotherm for the adsorption of Hg^{2+} on CeP (a) and CeP/Urea (b)

Conclusion

This study investigated the synthesis and characterization of fibrous nanocerium phosphate (CeP) and its urea intercalated analogue (CeP/Urea) followed by studying their efficiency in mercury ion (Hg^{2+}) adsorption. Characterization techniques (FTIR, XRD, SEM, TGA) confirmed successful synthesis.

Adsorption studies showed that contact time significantly affects efficiency, with about 98% mercury removal achieved within 20 minutes at pH 3. Increased initial mercury concentration correlated with higher adsorption capacity, but excess adsorbent reduced efficiency due to active site saturation.

Overall, findings emphasize optimizing adsorbent amount and solution conditions to enhance mercury removal. Urea intercalation improves cerium phosphate's structure, but careful dosage consideration is essential for maximizing capacity, aiding in the development of effective materials for heavy metal removal from water.

Conflict of interest:

The authors declare that there are no conflicts of interest

References

Abdel-Hady, E. E., Mohamed, H. F. M., Hafez, S. H. M., Fahmy, A. M. M., Magdy, A., Mohamed, A. S., Ali, E. O., Abdelhamed, H. R., & Mahmoud, O. M. (2023). Textural properties and adsorption behavior of Zn–Mg–Al layered double hydroxide upon crystal violet dye removal as a low cost, effective, and recyclable adsorbent. *Scientific Reports*, *13*(1). https://doi.org/10.1038/s41598-023-33142-x

Akl, Z. F. (2021). Theoretical and experimental studies on uranium(vi) adsorption using phosphine oxide-coated magnetic nanoadsorbent. *RSC Advances*, *11*(62), 39233–39244. https://doi.org/10.1039/d1ra04515f

Al-Ghouti, M. A., Da'ana, D., Abu-Dieyeh, M., & Khraisheh, M. (2019). Adsorptive removal of mercury from water by adsorbents derived from date pits. *Scientific Reports*, *9*(1). https://doi.org/10.1038/s41598-019-51594-y

AlHanash H. B., Issa R. A. M., and AlJabo H. A. (2022) Adsorption of UO_2^{2+}on Fibrous Cerium Phosphate and its Alanine and Arginine Intercalated Materials *Academic Journal of Chemistry*, *7*(4), 47-54, DOI: https://doi.org/10.32861/ajc.74.47.54

Aljamali N. M., Aldujaili R. A., Intisar Obaid Alfatlawi I. O. (2021) Physical and Chemical Adsorption and its Applications, *International Journal of Thermodynamics and Chemical Kinetics 2*(7),2456-6977.

BASH J. O, BRESNAHAN P, and MILLERD. R. (2007) Dynamic Surface Interface Exchanges of Mercury: A Review and Compartmentalized Modelling Framework, *Journal of applied meteorology and Climatology*, *46*, 1606-1617.

Boparai, H.K., Joseph, M., O'Carroll, D.M., (2011) Kinetics and thermodynamics of cadmium ion removal by adsorption onto nano zerovalent iron particles. *J. Hazard Mater*. *186*(1), 458–465. https://doi.org/10.1016/j.jhazmat.2010.11.029.

Deng, J., Zhang, X., Zeng, G., Gong, J., Niu, Q., Jie Liang, J., (2013) Simultaneous removal of Cd (II) and ionic dyes from aqueous solution using magnetic graphene oxide nanocomposite as an adsorbent, *Chem. Eng. J. 226, 189–200*, *http://dx.doi.org/10.1016/j.cej.2013.04.045*.

Doğan, M., Turhan, Y., Alkan, M., Namli, H., Turan, P., Demirbaş, (2008) Functionalized sepiolite for heavy metal ions adsorption, *Desalination*, *230*, 248–268.

Duan, W., Wang, J., Chang, L., Zhao, L., Tian, Z., Huanga, Z., and Huanga, W. (2018) Adsorption of mercury (II) from water by a novel sPAN fiber containing sulfhydryl, carboxyl and amino groups, *RSC Adv.*, *8*, 38259–38269, DOI: 10.1039/c8ra06998k.

Ebrahimi, S.J., Eslami, A., and Ebrahimzadeh, L. (2012) Evaluation of Heavy Metals Concentration in the Drinking Water Distribution Network in Kurdistan Villages, Research Journal of Pharmaceutical Biological and Chemical Sciences, *RJPBCS*, *6* (2), 55-61. https://www.researchgate.net/publication/282187333.

Zeng G., Li X., Huang J., Zhang C., Zhou C., Niu J. (2011) Micellar-enhanced ultrafiltration of cadmium and methylene blue in synthetic wastewater using SDS, *J. Hazard. Mater.*, *185*, 1304–1310, https://doi.org/10.1016/j.jhazmat.2010.10.046.

Gao, Y., Jiang, X., & Li, Z. (2023) Efficiency of Ion Exchange in Water Pollutant Removal: A Comprehensive Study. *Journal of Hazardous Materials*, *442*, 123153

Ghasemi, S. S., Hadavifara, M., Malekib, B., Mohammadniaa, E. (2019) Adsorption of mercury ions from synthetic aqueous solution using polydopamine decorated SWCNTs, *Journal of Water Process Engineering*, https://doi.org/10.1016/j.jwpe.2019.100965.

Guerra, D, L., Viana, R. R., and Airoldi, C. (2009) Adsorption of mercury cation on chemically modified clay, *Materials Research Bulletin*, *44*(3), 485-49, https://doi.org/10.1016/j.materresbull.2008.08.002

Issa R. A. M., El Amari A. O., AlHanash H. B. and Etmimi H. M. (2023) Removal of uranium (VI) ion from aqueous solution using kaolinite, *Kuwait Journal of Science*, *50*(4), 609-614, https://doi.org/10.1016/j.kjs.2023.03.010

Kumar, A., & Singh, P. (2021) Applications of Ion Exchange in Water and Wastewater Treatment. *Environmental Science and Pollution Research*, *28*(6), 6936-6949.

Langmuir, I., (1918) The adsorption of gases on plane surfaces of glass, mica and platinum. *J. Am. Chem. Soc.*,

40(9), 1361–1403. https://doi.org/10.1021/ja02242a004.

McKay G, Blair HS, and Gardner JR (1982) Adsorption of dyes on chitin, *J. Appl Polym Sci*, *27*(8), 3043-3057.

Michailidou, G., Koumentakou, I., Liakos, E. V., Lazaridou, M., Lambropoulou, D. A., Bikiaris, D. N., and Kyzas, G. Z., (2021) Adsorption of Uranium, Mercury, and Rare Earth Elements from Aqueous Solutions onto Magnetic Chitosan Adsorbents: A Review, Polymers (Basel), *13*(18): 3137, doi: 10.3390/polym13183137.

Perwitasari D,S, Pangestu M.A., Y.A Pracesa, Tola P. S., (2021), Langmuir and Freundlich Isotherm Approximation on Adsorption Mechanism of Chrome Waste by Using Tofu Dregs, *Nusantara Science and Technology Proceedings*, 2nd *International Conference Eco-Innovation in Science, Engineering, and Technology*, doi.org/10.11594/nstp.2021.1417

Qasem, N. A. A., Mohammed, R. H., & Lawal, D. U. (2021) Removal of heavy metal ions from wastewater: a comprehensive and critical review. *Npj Clean Water*, *4*(1). doi:10.1038/s41545-021-00127-0

Shakshooki S. K. (2014) Nano Fibrous Cerium(IV) Hydrogen Phosphate Membrane Self Supported Polymerization Agent, *J. Chem. Chem. Eng.*, *8*, 378-384.

Suleyman I. (2020) Sorption of europium on cerium phosphate using Box-Behnken design, *Turk J Chem.*, *44*,971-986.

Wang, Y., Zhang, G., and Liu, X. (2023) Ion-exchange behaviour of cerium-based nanomaterials for water treatment, *Environmental Science & Technology*, *55*(11), 5400-5404.

Youssif, M.M.; El-Attar, H.G.; Małecki, S.; Włoch, G.; Czapkiewicz, M.; Kornaus, K.; Wojnicki, M (2024) Mercury Ion Selective Adsorption from Aqueous Solution Using Amino-Functionalized Magnetic Fe_2O_3/SiO_2 Nanocomposite. *Materials*, *17*, 4254. https://doi.org/10.3390/ma17174254.

Zhangtao Li, Lu Wang, Jun Meng, Xingmei Liu , Jianming Xu, Fan Wang, Philip Brookes (2018) Zeolite-supported nanoscale zero-valent iron: New findings on simultaneous adsorption of Cd(II), Pb(II), and As(III) in aqueous solution and soil, *Journal of Hazardous Materials*, *344*, 1-11, https://doi.org/10.1016/j.jhazmat.2017.09.036.

Zhao, L., Chen, Q., & Zhang, Y. (2022) Environmental Benefits of Ion Exchange: Analysis and Perspectives. *Water Sustainability*, *12*(3), 455-467.